Environmental Science and Pollution Research (2022) 29:25748–25758
https://doi.org/10.1007/s11356-021-17501-7

RESEARCH ARTICLE

High-efficiency adsorption of Cd(II) and Co(II) by ethylenediaminetetraacetic dianhydride-modified orange peel as a novel synthesized adsorbent

Fanghui Wang[1,2] · Peng Wu[1,2] · Lin Shu[1,2] · Di Huang[3] · Huanhuan Liu[1,2]

Received: 9 August 2021 / Accepted: 8 November 2021 / Published online: 30 November 2021

Abstract

The treatment of heavy metal (HM) wastewater is a critical and considerable challenge. Fruit peel-based HM adsorption is a promising way for the water pollution control and the reuse of agricultural waste. In this study, a novel adsorbent based on orange peel was synthesized for the first time by introducing abundant -COO groups with ethylenediaminetetraacetic dianhydride (EDTAD) to eliminate Cd(II) and Co(II) of sewage solution. The synthesized adsorbent displayed excellent adsorption capacity of 51.020 and 40.486 mg/g for Cd(II) and Co(II), respectively, and the adsorption equilibrium was achieved within 5 min, following the Langmuir isotherm model and the pseudo-second-order model. Surface characterization of adsorbents by scanning electron microscopy-energy dispersive X-ray spectroscopy, Fourier transform infrared spectroscopy, and X-ray photoelectron spectroscopy confirmed that ion exchange, complexation, and physical adsorption could occur during the adsorption process. The rapid and highly efficient adsorption performance suggests EDTAD-modified synthesized orange peel possesses great potential for HM removal from sewage systems.

Keywords EDTAD · Orange peel · Adsorption · Heavy metal · Sewage systems

Introduction

Environmental pressure has always been an important problem for human health with the rapid growth of global economics (Annadurai et al. 2003; Gupta et al. 2018; Villen-Guzman et al. 2021). Soil and water pollution of heavy metals (HMs) has become widespread worldwide due to human activities, including the excessive use of metal-based fertilizers manures and farm chemicals in agricultural practices, metallurgical engineering, urban sewage discharges, intensive soil development, and metal mining activities (Gu et al. 2014; Anju and Banerjee, 2011; Zhang et al. 2019a). Due to the non-biodegradability, HMs tend to be accumulated in water bodies (Ayoubi and Karami 2019, Jia et al. 2020, Tan et al. 2016, Yong et al., 2020), and then the ecosystem is seriously damaged by reducing water quality and biological transmission and enrichment (Bulin et al. 2020, Kerr and Cooke, 2017). Among the HMs, cobalt (Co(II)) and cadmium (Cd(II)) are both considered the most common pollutants in many industrial applications, and they are also important factors affecting human healthy. These HMs are chronic in the human body and may cause carcinogenic and non-carcinogenic

Responsible Editor: Tito Roberto Cadaval Jr

Fanghui Wang and Peng Wu contributed equally to this work

✉ Di Huang
huangdi@nankai.edu.cn

✉ Huanhuan Liu
lh_tust@tust.edu.cn

Fanghui Wang
19846023@mail.tust.edu.cn

Peng Wu
18845005@mail.tust.edu.cn

[1] State Key Laboratory of Food Nutrition and Safety, Tianjin University of Science & Technology, Tianjin 300457, China

[2] Key Laboratory of Food Nutrition and Safety, Ministry of Education, Tianjin University of Science & Technology, Tianjin 300457, China

[3] TEDA School of Biological Sciences and Biotechnology, Nankai University, TEDA, Tianjin 300457, China

toxic effects (Brohi et al. 2021; Ma et al. 2017; Sameena et al. 2019). It is reported that Cd can trigger femoral pain, sterility, renal injuries, and immune deficiencies (Memon et al. 2008); excessive intake of Co gives rise to neurotoxicity (Singh and Shukla, 2015). Therefore, the protection of surface water and groundwater has become an important task at present. Equally, those HMs which were already discharged in a reasonable way must be managed to reduce the emission.

In order to deal with the pollution of HMs, various treatment measures have been put into effect, including but not limited to ion exchange, coagulation, solvent extraction, chemical precipitation (Németh et al. 2016), membrane filtration (Fang et al. 2017), and electrochemical treatment (Mourya et al. 2019). While effective adsorption performances have been achieved, some critical shortcomings still exist, such as high energy consumption and secondary pollution. More important, most of these procedures are expensive and complicated, thus offsetting their advantages (Kai et al. 2017, Li et al. 2018).

To overcome these limitations, the strategy of biosorption, as a powerful method to efficiently remove HMs from sewage system, has been widely used in the construction of efficient, simple, and inexpensive platforms in recent years (Jurado-Sánchez et al. 2015; Mia et al. 2017). For example, Jin et al. isolated endophytic fungi from plants to cope with HMs contamination (Jin et al. 2019). Módenes et al. evaluated the biosorption of HMs by dead plant macrophyte *Egeria densa* in fixed bedposts (Módenes et al. 2018). Agricultural and food industry wastes, such as grapefruit, straw, and seed bark, have also proved to be effective to remove HMs by adsorption (Jin et al. 2018).

As the world's largest fruit producing country, China generates approximately 31.98 million tons of fruit waste every year (Pathak et al. 2015). Among them, orange peel is rich in lignin, cellulose, hemi-cellulose, and pectin that contain various functional groups (-OH, -COOH, etc.), which is suitable for large-scale preparation of renewable adsorbents to deal with HMs (Vilardi et al. 2018). However, the low adsorption efficiency of raw orange peel on HMs is still unsatisfactory, and many chemical modification methods have been tried to enhance the capture ability. For example, the maximum removal capacities of Cd(II) and Co(II) by using orange peel modified with nitric acid were 13.70 and 1.82 mg/g, respectively (Annadurai et al. 2003; Lasheen et al. 2012), whereas the adsorption capacity of Cd(II) by the grafted copolymerization-modified, HNO_3-modified, and active carbon orange peels were 21.53, 11.20, and 28.67 mg/g (Feng et al. 2011, Lasheen et al. 2012, Moreno-Pirajan and Giraldo, 2012). Still, the time required to reach equilibrium was at least 0.5 h. These studies suggest that orange peel is a promising adsorbent, but the adsorption capacity needs to be strengthened.

Ethylenediaminetetraacetic dianhydride (EDTAD) is an efficient derivatization reagent for chelating metal ions, which contains two anhydride groups per molecule. Abundant carboxyl functional groups with high capacity to form stable complexes with HMs can be introduced into biomass materials through esterification reaction (Chen et al. 2012; Kołodyńska et al. 2008). The excellent features of EDTAD facilitate us to develop a facile method to manufacture a new adsorbent with superior adsorption capacity for HMs. In this regard, orange peel was chemically modified by EDTAD for the first time through esterification reaction, and a large number of -COO groups were introduced, which have been proposed for Cd(II) and Co(II) removals. The specific aims of the work are (1) using EDTAD to modify biomaterial to improve its adsorption performance for HMs; (2) investigating the effects of pH, initial concentration and contact time of HMs, and competitive adsorption of Cd(II) and Co(II) loaded on material, as well as the adsorption kinetics, isotherms, and thermodynamics; (3) characterizing the desired material using SEM, EDX, FT-IR, and XPS to reveal the physical and chemical properties of the adsorbents; and (4) elucidating the underlying adsorption mechanisms.

Materials and methods

Materials

Orange peel used in the study was collected from the local market originating from Nanning, Guangxi Province, which was the famous orange-producing area of China. The peel was first washed for four times and dried at 50 ℃ to constant weight, then cut into small pieces about 1 cm, and crushed and sieved with 40 mesh Taylor screen.

N–N-dimethylformamide (DMF, purity 99.5%) and ethylenediaminetetraacetic dianhydride (EDTAD, purity 95%) were provided by Thermo Fisher Scientific Co. ltd; high purity (≥9 9.9%) $Cd(NO_3)_2$ and $Co(NO_3)_2$ were provided by Shanghai Macklin Biochemical Co., Ltd., China. The rest of reagents were purchased from Shanghai Sinopharm Chemical Reagent Co., Ltd., China. The water used in this experiment was purified through the Milli-Q water purification system (Millipore, USA).

Adsorbent preparation

Degreasing and deproteinization of peels

According to the previous method, the peel was defatted by Soxhlet extraction method for 5 h with N-hexane and ethanol (1:1) to remove the lipids (Júnior et al. 2009) and then deproteinized to expose the hydroxyl groups for the esterification reaction, which were operated by mixing with

NaOH solution (5 M) over night to obtain mercerized peels, repeating twice and generating secondary mercerized peels defined as modified orange peel (MOP).

Preparation of EDTAD-modified peels

Peraira's method was used to prepare the EDTAD-modified material with some changes (Pereira and Gurgel, 2010). Briefly, MOP was mixed with EDTAD (1:1.5, w/w) in 42 ml DMF and continuously stirred for 20 h at 75 ℃ and then centrifuged at 10,000 × *g*. The precipitate was washed with DMF, deionized water, saturated $NaHCO_3$, deionized water, 95% ethanol aqueous solution, and acetone in turn. The precipitate was dried in room temperature to obtain EDTAD-modified orange peel (EMOP).

Adsorption experiments

The standard storage solutions of Cd(II) and Co(II) (500 mg/L) were prepared by dissolving $Cd(NO_3)_2$ and $Co(NO_3)_2$ into deionized water and calibrating the concentration by inductively coupled plasma-atomic emission spectroscopy (ICP-OES, Avio 200, PerkinElmer, USA) (Zhang et al. 2020b). All other concentrations used in this study were serial dilutions from stock solutions. The adsorbent and the standard HM solutions were placed in a 200-rpm shaker at a ratio of 1 mg:1 ml at room temperature for adsorption experiments. Subsequently, the solid liquid mixtures were separated by centrifugation at 10,000 × *g* and passed through a 0.22-μm Nylon filter. The dried adsorbent was then adapted for subsequent FT-IR, SEM–EDX, and XPS analysis. Specifically, single-factor experiments were applied to investigate the effects of pH (3–7), initial metal ion concentration (30–250 mg/L for Cd and 20–150 mg/L for Co), and contact time (1–180 min) on the removal process. The pH of ionic solutions was adjusted with 1 M HCl or NaOH solutions, and the equilibrium adsorption capacity of the adsorbent was expressed by Eq. (1):

$$Q_e = \frac{(C_0 - C_e)V}{W} \quad (1)$$

where Q_e is the equilibrium adsorption capacity (mg/g), C_0 and C_e are the initial and equilibrium ion concentrations (mg/L), V is the solution volume (L), and W is the weight of the adsorbent (g).

Characterization of the adsorbents

Semi-quantitative elemental analysis of EMOP surface morphology observation by using field emission high-resolution scanning electron microscope (SEM; Apeo, FEI Inc., USA) combined with energy dispersive X-ray spectroscopy (EDX) was performed (Zhang et al. 2018). Fourier transform infrared spectra (FT-IR) spectra using KBr pressed disk technique were determined on a FT-IR spectrometer (IS 50, Thermo) (Huang et al. 2019). Surface element composition and atomic valence of EMOP were detected by X-ray photoelectron spectroscopy (XPS; ESCALAB 250Xi, Thermo Fisher Scientific Inc., USA) (Ding et al. 2020). The C1s peak at 284.8 eV was used as the standard for calibration.

Results and discussion

Modification of orange peel improved HMs removal capacity

The adsorption capacity of modified material for metal ions has been significantly improved (Fig. 1). For the unmodified orange peel (UOP), the removal capacity for Cd(II) and Co(II) was limited, only 12.60 and 7.58 mg/g, while the adsorption capacity for mercerized orange peel (MOP) was 19.86 and 12.10 mg/g, respectively, both of which were far behind that of modification with EDTAD (EMOP, 40.45 and 22.89 mg/g). Interestingly, whether modified or not, the orange peel had better adsorption performance on Cd(II) than Co(II).

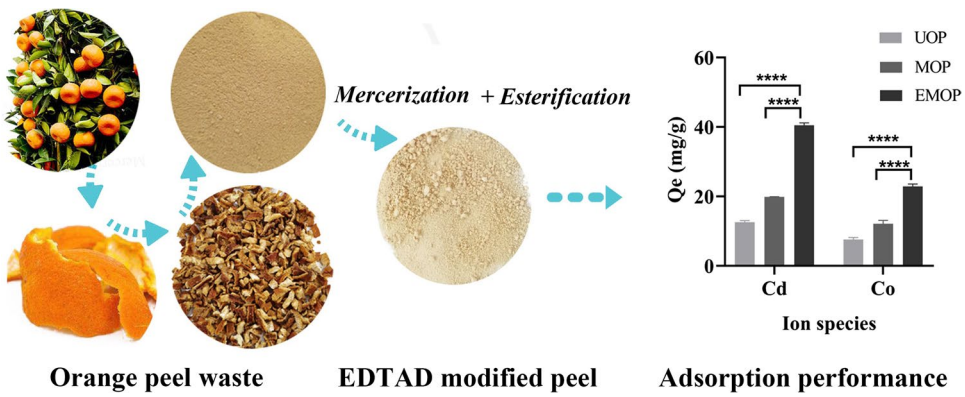

Fig. 1 The fabrication of EDTAD-modified material composite. After cutting, drying, and crushing, the orange peel modified by EDTAD was obtained by mercerization and esterification. Adsorbent dose = 1 g/L, C_0 is 70 mg/L for Cd and 50 mg/L for Co, t = 3 h, T = 25 °C, r = 200 rpm. ****$p < 0.0001$

Effect of initial pH

The initial pH of the solution was a key parameter affecting the adsorbate characteristics and the surface properties of the adsorbent material. As shown in Fig. 2a, the extremely low level of adsorption occurred at pH 3.0, which might be caused by the strong competition between H(I) and HMs for binding sites (Bulin et al. 2020; Surgutskaia et al. 2020). With the increase of pH, the adsorption capacity of the adsorbent on HMs improved from 3.0 to 5.0 and then reached a plateau region between 5.0 and 7.0, possibly because the concentration of H(I) in the solution decreased, weakening the competition with HMs for binding sites.

Adsorption isotherms

To comprehend the adsorption process and the relationship between adsorbent and HMs, the adsorption isothermal experiments were performed at 25 ℃ by changing the initial concentrations of Cd(II) (30–250 mg/L) and Co(II) (20–150 mg/L). The Langmuir (Eq. (2)) and Freundlich (Eq. (3)) isotherm models were utilized to analyze the adsorption type of surface coverage the adsorption belonged to and estimate the maximum adsorption capacity (Chen et al. 2021). The Langmuir isotherm is assumed that adsorption process occurs at a specific uniform location in the adsorbent, and the Freundlich isotherm is not confined to a monolayer adsorption, which explains the reversible heterogeneous surface (Bagheri et al. 2021). The equations (Elkady et al. 2020) for these models are as follows:

$$Q_e = \frac{Q_m K_c C_e}{C_e K_c + 1} \quad (2)$$

$$Q_e = C_e^{1/n} + K_f \quad (3)$$

where Q_m is the maximum adsorption capacity (mg/g), K_c is Langmuir constant associated with energy of adsorption (L/mg), and K_f ($L^{1/n}$ $mg^{1-1/n}$ g^{-1}) and 1/n are Freundlich constants related to adsorption capacity and intensity, respectively.

The curve of adsorption capacity versus initial concentration was shown in Fig. 2b. Obviously, as the initial concentration increased, the adsorption capacity increased until reached a critical value, where the adsorption tended to be saturated. It was evidently that the Langmuir model ($R_L^2 = 0.995–0.999$) was fitted better to the Cd(II) or

Table 1 Parameters of the Langmuir and Freundlich isotherm models in single HMI system under different initial concentrations and kinetic parameters for the removal of Cd(II) and Co(II) on adsorbents

Metal ion		Cd(II)	Co(II)
Langmuir parameters	Q_m (mg/g)	51.020	40.486
	K_C (L/mg)	0.080	0.063
	R_L^2	0.995	0.999
Freundlich parameters	K_F ($L^{1/n}$ $mg^{1-1/n}$ g^{-1})	25.386	0.298
	1/n	0.122	1.119
	R_F^2	0.801	0.464
Pseudo-first-order	Q_e (mg g^{-1})	4.513	2.762
	K_1 (g min^{-1} mg^{-1})	0.022	0.011
	R_1^2	0.953	0.852
Pseudo-second order	Q_e (mg g^{-1})	41.152	21.097
	K_2 (g min^{-1} mg^{-1})	0.219	1.404
	R_2^2	0.993	0.991
Intra-particle diffusion	K_{id} (mg g^{-1} $min^{-0.5}$)	5.106	2.529
	C	28.893	17.345
	R_3^2	0.999	0.999

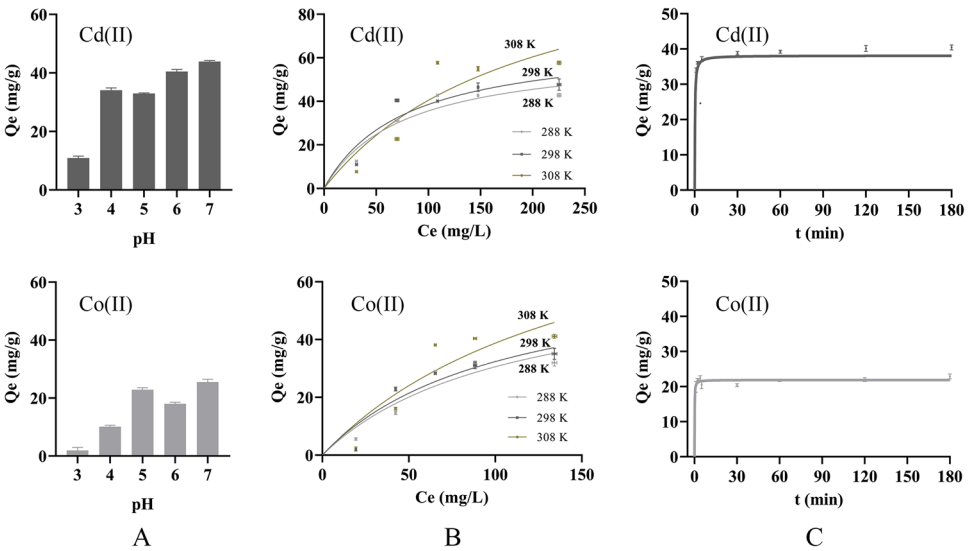

Fig. 2 The effects of solution pH, initial concentration, contact time on adsorption capacity. **a** Orange peel under different pH. Adsorbent dose = 1 g/L, C_0 is 70 mg/L for Cd and 50 mg/L for Co, t = 3 h, T = 25 °C, r = 200 rpm. **b** Initial concentrations under different temperatures. Adsorbent dose = 1 g/L, t = 3 h, T = 25 °C, r = 200 rpm. **c** Contact time at optimal pH. Adsorbent dose = 1 g/L, t = 1–180 min, C_0 is 70 mg/L for Cd and 50 mg/L for Co, T = 25 °C, r = 200 rpm

Co(II) adsorption by EMOP than the Freundlich model ($R_L{}^2 = 0.464–0.801$) (Table 1), which demonstrated that the adsorption was single-layer and homogeneous (Yuan et al. 2017). The Q_e of Cd(II) and Co(II) computed via Langmuir model were 51.020 and 40.486 mg/g, respectively. Especially worthy of attention, the Q_e of Cd(II) and Co(II) on EMOP in this work was significantly higher than previous studies (ranged from 1.82 to 13.70 mg/g) (Annadurai et al. 2003; Lasheen et al. 2012), suggesting that EDTAD modification was a suitable strategy for preparing adsorbents to remove Cd(II) and Co(II) from the sewage systems.

Adsorption kinetics

To probe the adsorption kinetics of Cd(II) and Co(II) onto EMOP, the adsorption capacity of Cd(II) and Co(II) were detected within specified time intervals. Figure 2c showed the changes of adsorption capacity over time. The adsorption rate was extremely fast in the initial stage and reached equilibrium within 5 min, much more efficient than previous studies (at least 30 min) (Chen et al. 2021; Gao et al. 2019; Liu et al. 2012; Zheng et al. 2020).

In addition, the pseudo-first-order (Eq. (4)) and the pseudo-second-order (Eq. (5)) models were employed to calculate the adsorption capacity of Cd(II) and Co(II) on EMOP and reveal the removal mechanism. The pseudo-first-order model describes the mass transfer between the adsorbent and the metal ions, dominated by the physical adsorption; the pseudo-second-order model representatives the chemical adsorption (Antuna-Nieto et al. 2020). These equations are as follows:

$$Q_t = Q_e(1\text{-}e^{-K_1 t}) \tag{4}$$

$$Q_t = \frac{k_2 Q_e^2 t}{1 + K_2 Q_e t} \tag{5}$$

where Q_t (mg/g) is the adsorption capacity at t, and K_1 (g mg^{-1} min^{-1}) and K_2 (g mg^{-1} min^{-1}) are the adsorption rate constants of pseudo-first-order and pseudo-second-order, respectively.

The corresponding parameters of kinetic models obtained in the adsorption experiments were showed in Table 1. Obviously, the R^2 of the pseudo-second-order model for Cd(II) and Co(II) were 0.993 and 0.991, respectively, which exhibited a higher adaptation than the pseudo-first-order model for Cd(II) (0.953) and Co(II) ($R^2 = 0.852$). And the adsorption capacity calculated theoretically obtained by the pseudo-second-order model of Cd(II) and Co(II) were closer to the experimental data, suggesting that the loading of Cd(II) and Co(II) by adsorbent was dominated by chemisorption rather than physical performance (Yang and Jiang 2014).

To explore whether the intra-particle diffusion was a rate-limiting step, an intra-particle diffusion model was adopted to expound the porous network and active binding sites of HMs diffusing from the solution to the adsorbent (Cabooter et al. 2021). The data were well fitted to the intra-particle diffusion model ($R^2 = 0.999$), but the linear plots did not pass the origin, indicating that the capture process for Cd(II) and Co(II) was possibly governed both by the intra-particle diffusion and physical adsorption (Zhang et al. 2020a). The adsorption equilibrium was finally achieved within 5 min due to the saturation of the adsorption sites and the decline of Cd(II) and Co(II) concentration:

$$Q_t = K_{id} t^{0.5} + C \tag{6}$$

where K_{id} (mg g^{-1} $min^{-0.5}$) is the constant of intra-particle diffusion and C represents a constant associated with boundary thickness.

Adsorption thermodynamics

In this study, Gibbs energy change (ΔG), enthalpy change (ΔH), and entropy change (ΔS) were calculated for adsorption thermodynamics study. The relationship between them was as follows (Behjati et al. 2018):

$$\triangle G = -RT\ln K_e = -RT\ln\left(Q_e/C_e\right) = \triangle H - T \triangle S \tag{7}$$

In Fig. 2b, Q_e gradually increased as the temperature increased. The thermodynamic parameters of Cd(II) and Co(II) adsorption by EMOP were listed in Table 2. The values of ΔG were all negative and decreased with temperature, indicating that the adsorption of Cd(II) and Co(II) by EMOP were spontaneous and thermodynamically favorable process. The positive ΔH values suggested that the adsorption of Cd(II) and Co(II) by EMOP was endothermic, and higher temperature was beneficial to this process. Moreover, the positive ΔS values meant an increase in the randomness of the solid–liquid interface after Cd(II) and Co(II) adsorption, and the adsorption was favorable (Xu et al. 2021).

Table 2 Thermodynamic parameters for the removal of Cd(II) and Co(II) on adsorbents. Adsorbent dose = 1 g/L, C_0 is 200 mg/L for Cd and 140 mg/L for Co, t = 3 h, r = 200 rpm

	T (K)	ΔG (kJ·mol^{-1})	ΔH (kJ·mol^{-1})	ΔS (J·mol^{-1}·K^{-1})
Cd(II)	288	−2394.1	4.386	8.328
	298	−2477.3		
	308	−2560.6		
Co(II)	288	−504.17	2.687	1.760
	298	−521.77		
	308	−539.37		

Mixed competitive adsorption

For the purpose of comparing the adsorption effects of EMOP on Cd(II) and Co(II), mixed adsorption experiments were performed. From Fig. 3, we can see that the loading capacity for Cd(II) was stronger than Co(II) in the mixed HM solution, indicating that EMOP exhibited higher adaptability to Cd(II), which was similar to previous result (Li et al. 2008). Furthermore, the total adsorption capacity of the mixed ion solution was close to the maximum adsorption capacity of the single ion, indicating that the adsorption reached saturation state.

Desorption and reusability

As shown in Fig. 4a, generally, desorption efficiency decreased with pH and then stabilized from pH 4.0 to 6.0. For Cd(II), the maximum desorption efficiency was 90.58% at pH 1.0, while 93.94% for Co(II), suggesting the adsorbent of EMOP might be easily regenerated by HCl treatment (Kołodyńska et al. 2017). HCl was chosen as the regeneration reagent in the reusability experiment, and the removal rate of Cd(II) and Co(II) was displayed in Fig. 4b. The removal rate of Cd(II) and Co(II) by EMOP decreased to 53.97% and 40.85% after 3 times of adsorption–desorption cycle. The decrease of removal efficiency may be ascribed to the block of pore structure and decrease of iron binding sites (Mei et al. 2021).

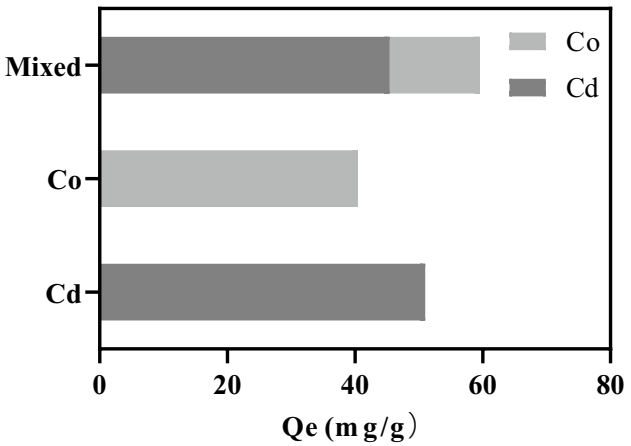

Fig. 3 Comparison of the mixed ion adsorption and the single ion adsorption. Adsorbent dose = 1 g/L, pH = 6, t = 3 h, C_0 of each HM is 100 mg/L, T = 25 °C, r = 200 rpm

Adsorption mechanisms

Various characterizations including SEM–EDX, FT-IR, and XPS were integrated to analyze the mechanisms of the adsorption process of Cd(II) and Co(II) on EMOP. Obviously, the surface of the unmodified orange peel (UOP) was comparatively smooth (Fig. 5a, b), but the surface of EDTAD-modified peel (EMOP) presented a loose and porous structure and became shrunken, which provided more adsorption sites for Cd(II) and Co(II). Such changes might be attributed to the removal of lipids and proteins during the mercerization treatment. The EDX spectrum was performed to determine whether Cd(II) and Co(II) were successfully adsorbed to the peel surface and explore element changes before and after modification. After modification, the disappearance of P and K in the peel and the introduction of Na fully indicated that the material has been successfully modified (Fig. 5c, d). When adsorption reaction was completed, it was evident that ions were successfully adsorbed because Cd and Co appeared on the material surface (Fig. 5e). In addition, it was obvious from Fig. 5e that the content of Na element was significantly reduced, indicating that ion exchange occurred in the adsorption process (Júnior et al. 2009).

To further understand the surface characteristics of EMOP and its adsorption mechanism for Cd(II) and Co(II), FT-IR was carried out, and the spectra was depicted in

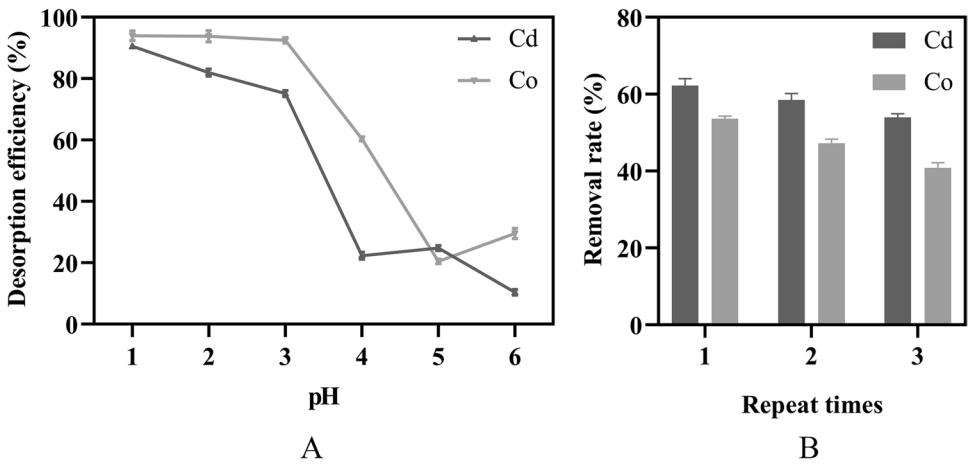

Fig. 4 Desorption and recycling of Cd(II) and Co(II) on EMOP. **a** Desorption efficiency under different pH. Adsorbent dose = 1 g/L, C_0 is 70 mg/L for Cd and 50 mg/L for Co, t = 3 h, T = 25 °C, r = 200 rpm. **b** Removal rate of EMOP to Cd(II) and Co(II) under different repeat times. Adsorbent dose = 1 g/L, C_0 is 70 mg/L for Cd and 50 mg/L for Co, pH = 1, t = 3 h, T = 25 °C, r = 200 rpm

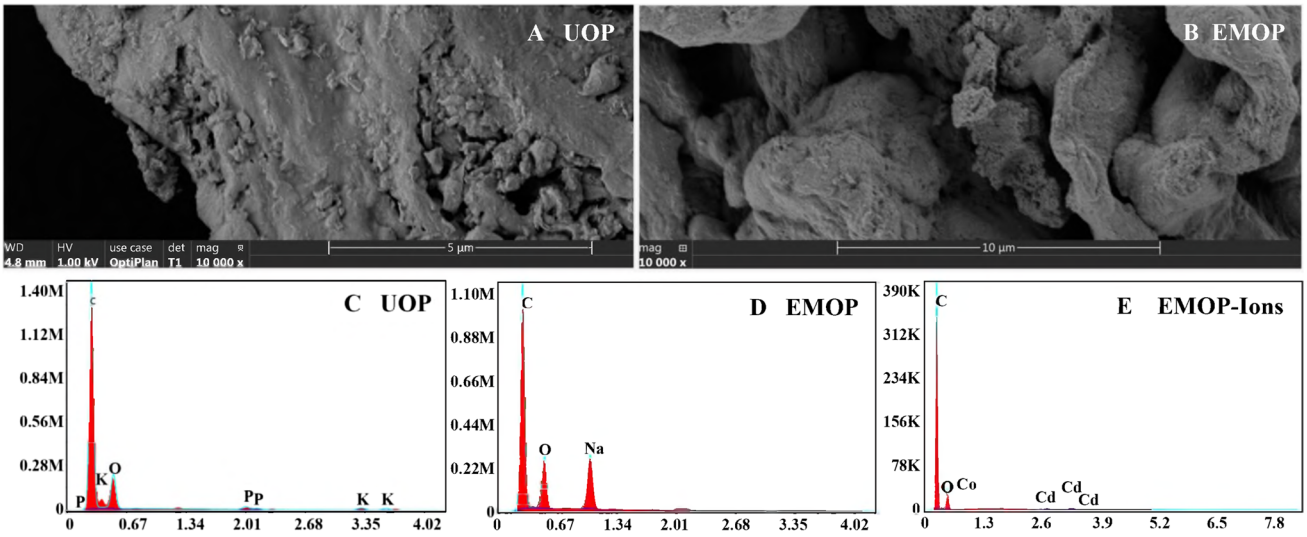

Fig. 5 Surface morphology and metal ions of the adsorbents observed by SEM–EDX. SEM: **a** UOP, unmodified orange peel; and **b** EMOP, EDTAD-modified orange peel. EDX: **c** Unmodified orange peel, **d** modified orange peel before adsorption, and **e** modified orange peel after adsorption

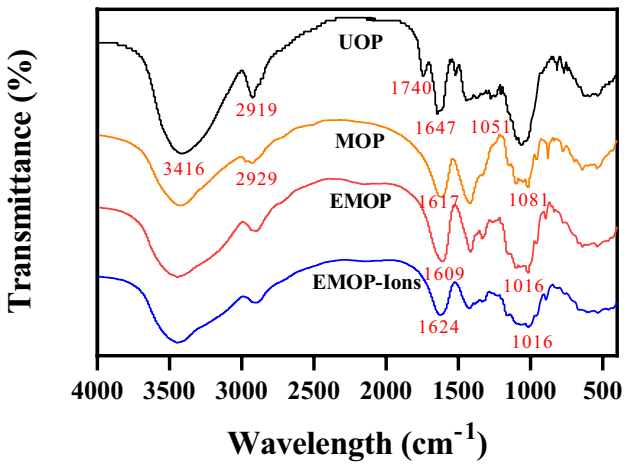

Fig. 6 FT-IR spectra of adsorbents before and after adsorption. UOP, unmodified orange peel; MOP, mercerized orange peel; EMOP, EDTAD-modified orange peel; EMOP-Ions, EDTAD-modified orange peel after adsorbing Cd and Co

Fig. 6. The signal around 3416 cm^{-1} attributed to the -OH stretching vibration; the peaks at 2919 and 2929 cm^{-1} could be ascribed to the asymmetric and symmetric C-H stretching, and the sharp peaks at 1647, 1617, 1609, and 1624 cm^{-1} represented the stretching of C = O, whereas 1051, 1081, and 1016 cm^{-1} were associated with C-O stretching (Lessa et al. 2017; Wang et al. 2014). It needed to be pointed out that the broader and weaker peaks assigned to C-H, C = O, and C-O were detected for MOP than UOP and the band at 1740 cm^{-1} which was ascribed to N–H stretching disappeared for MOP, indicating that the success of degreasing and deproteinization after mercerization (Krylova and Dukštienė, 2019, Zhang et al. 2018). The decrease of -OH peak and the increase of C = O and C-O peaks in EMOP just indicated that the adsorbent was successfully conjugated by EDTAD, and the -OH was substituted to introduce -COO group, which was one of the reasons for the significantly improved adsorption performance. After binding with HMIs, the decrease of peak intensity around 3416, 1624, and 1016 cm^{-1} and the blue shift from 1609 to1624 cm^{-1}, which could be attributed to the interaction between high electron density of metal ions and -COO group (Ding et al. 2016; Lim et al. 2008) illustrates the interaction between oxygen-containing groups (-OH, C = O,C-O, etc.) and HMs.

To explore the element types and atomic chemical valences on the surface of the material before and after adsorption, XPS analysis was performed. The full-spectrum and fine-spectrum scanning of C, O, Na, Cd, and Co before and after adsorption was displayed in Fig. 7. New characteristic peaks of Cd 3d (412.6 eV and 405.8 eV) and Co 2p (786.1 eV and 781.4 eV) appeared in the EMOP after adsorption, which indicated that Cd(II) and Co(II) were indeed captured. Additionally, the intensity of Cd 3d was stronger than that of Co 2p, supporting the finding that the orange peel has better adsorption performance on Cd(II) than Co(II). Even more noteworthy was the peak strength of Na 1 s around 1071.5 eV decreased after adsorption, manifesting that ion exchange might occur between Na(I) with Cd(II) and Co(II), which confirmed the EDX results. The C 1 s peaks of EMOP were split into three peaks at 284.8/284.8, 286.4/286.6, and 288.1/288.3 eV, representing C − C/C = C, C − O, and C = O, respectively (Zhang et al. 2019b). The binding energy of C-O and C = O in C 1 s shifted towards the higher binding energy by approximately

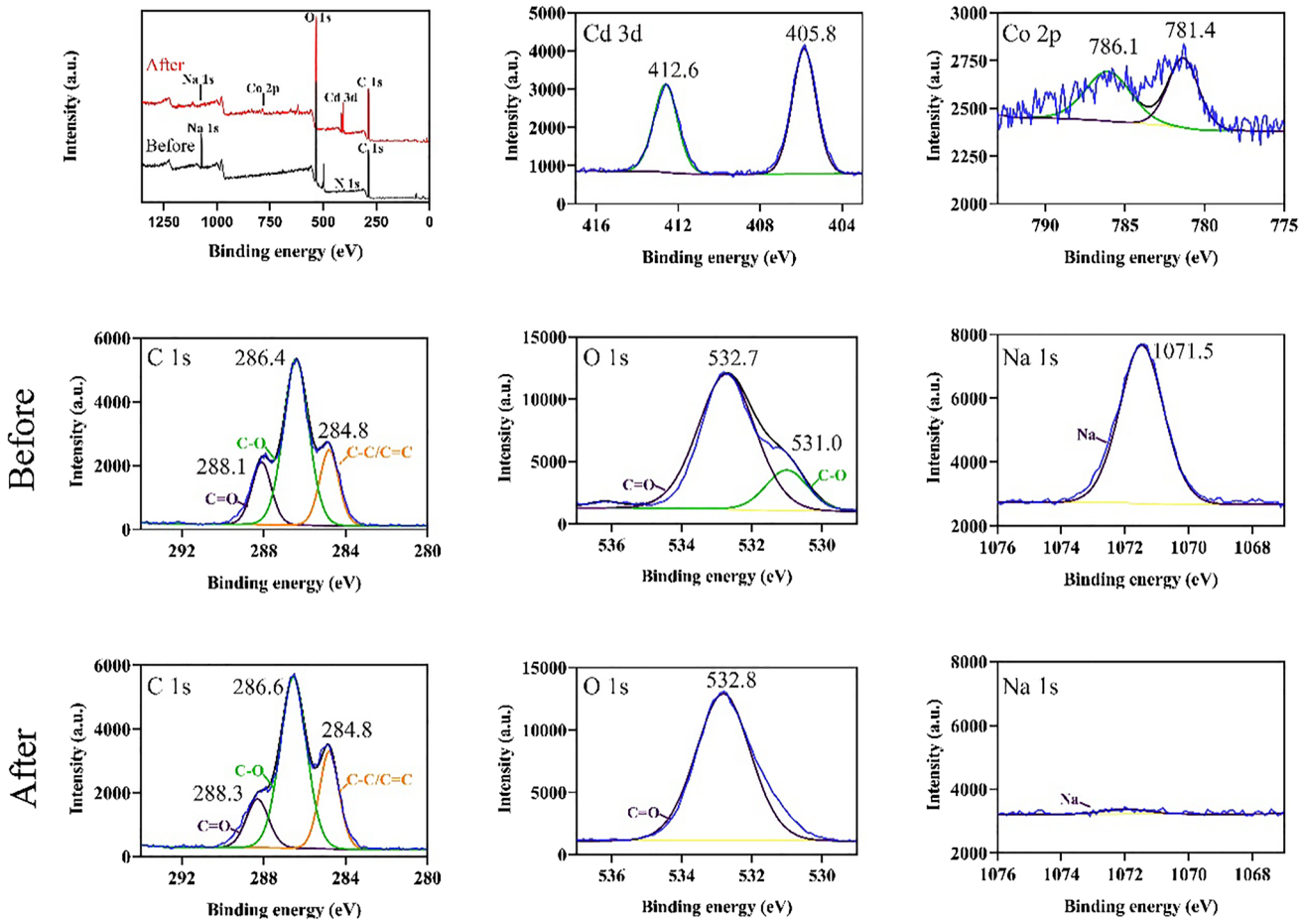

Fig. 7 High-resolution XPS spectra of adsorbents

0.2 eV, and the strength of C = O was notably decreased after adsorption, which might be caused by the complexation reaction between the ions and the oxygen-containing groups of EMOP. The O atom provided a lone pair electron to form a coordinated covalent bond with metal ions, which led to the decrease of O charge density and the increase of photoelectron binding energy (Ling et al. 2013; Zhao et al. 2013; Zhu et al. 2012). The O 1 s peaks were split into two major peaks, which were ascribed to C – O at 531.0 eV and C = O at 532.7/532.8 eV (Zhang et al. 2019b). The disappearance of C-O and the shift of C = O binding energy indicated that the binding between ions and EMOP preferred at the O atoms of C-O (Lim et al. 2008; Zhou et al. 2018).

Based on the above analysis, ion exchange, surface complexation, and physical adsorption may simultaneously participate in the adsorption process, in which chemical adsorption was dominant. Specifically, the decrease of Na peak strength in EDX and XPS indicated that free HMs may be replaced by –COO···Na···COO–. The change of -OH and -COOH in FT-IR and the shift of the C-O and C = O peak positions in XPS confirmed that complexation reactions occurred between the abundant oxygen-containing groups on the surface of EMOP and HMs to form C–O–Cd/Co complexes, which was consistent with previous work (Zhang et al. 2020c). In addition, the pore size and shrinkage structure of adsorbent surface indicated that physical adsorption may also be involved in the adsorption process.

Conclusion

To sum up, mercerization and esterification approach were utilized to transform orange peel into EDTAD-modified adsorbent in this study. The as-prepared EMOP had outstanding Cd(II) and Co(II) loading capabilities of 51.020 and 40.486 mg/g, respectively, and excellent kinetic performance (within 5 min), fitting with the pseudo-second-order and Langmuir isotherm model. The adsorption performance of EMOP might be attributed to abundant oxygen-containing groups since ion exchange and surface complexation were proved to be the main adsorption mechanism, which was assisted by physical adsorption. It can be concluded that

EDTAD-modified orange peel is a promising and environmentally friendly bio-adsorbent to treat HM pollution.

Acknowledgements We gratefully acknowledge the technical supports from Instrument & Testing Center of Tianjin University of Science and Technology.

Author contribution Fanghui Wang, conceptualization, investigation, data curation, and writing—original draft. Peng Wu, investigation, methodology, and writing—original draft. Lin Shu, investigation and review. Di Huang, conceptualization, supervision, and funding acquisition. Huanhuan Liu, conceptualization, supervision, writing—original draft, and funding acquisition.

Funding This work was supported by the National Natural Science Foundation of China (Grants 31800072, 31970084, 31400081) and the Open Fund of the Ministry of Education Key Laboratory of Molecular Microbiology and Technology, Nankai University.

Availability of data and materials The datasets used and/or analyzed during the current study are available from the corresponding author on reasonable request.

Declarations

Ethics approval and consent to participate Not applicable.

Consent for publication Not applicable.

Competing interests The authors declare no competing interests.

References

Anju M, Banerjee DK (2011) Multivariate statistical analysis of heavy metals in soils of a Pb–Zn mining area. Environmental Monitoring and Assessment, India. https://doi.org/10.1007/s10661-011-2255-8

Annadurai G, Juang RS, Lee DJ (2003) Adsorption of heavy metals from water using banana and orange peels. Water Sci Technol. https://doi.org/10.1016/S0043-1354(02)00272-5

Antuna-Nieto C, Rodriguez E, Lopez-Anton MA, Garcia R, Martinez-Tarazona MR (2020) Noble metal-based sorbents: a way to avoid new waste after mercury removal. J Hazard Mater. https://doi.org/10.1016/j.jhazmat.2020.123168

Ayoubi S, Karami M (2019) Pedotransfer functions for predicting heavy metals in natural soils using magnetic measures and soil properties. J Geochem Explor. https://doi.org/10.1016/j.gexplo.2018.12.006

Bagheri N, Mansour Lakouraj M, Hasantabar V, Mohseni M (2021) Biodegradable macro-porous CMC-polyaniline hydrogel: synthesis, characterization and study of microbial elimination and sorption capacity of dyes from waste water. J Hazard Mater. https://doi.org/10.1016/j.jhazmat.2020.123631

Behjati M, Baghdadi M, Karbassi A (2018) Removal of mercury from contaminated saline wasters using dithiocarbamate functionalized-magnetic nanocomposite. J Environ Manage. https://doi.org/10.1016/j.jenvman.2018.02.052

Brohi ROZ, Khuhawar MY, Mahar RB, Ibrahim MA (2021) Novel bimetallic nano particles for sorption of mercury (II) from drinking water: adsorption experiment and computational studies. Journal of Water Process Engineering. https://doi.org/10.1016/j.jwpe.2020.101727

Bulin C, Zhang Y, Li B, Zhang B (2020) Removal performance of aqueous Co(II) by magnetic graphene oxide and adsorption mechanism. J Phys Chem Solids. https://doi.org/10.1016/j.jpcs.2020.109483

Cabooter D, Song H, Makey D, Sadriaj D, Dittmann M, Stoll D, Desmet G (2021) Measurement and modelling of the intra-particle diffusion and b-term in reversed-phase liquid chromatography. J Chromatogr A. https://doi.org/10.1016/j.chroma.2020.461852

Chen X, Chen W, Mulchandani A, Mohideen U (2012) Application of displacement principle for detecting heavy metal ions and EDTA using microcantilevers. Sens Actuators, B Chem. https://doi.org/10.1016/j.snb.2011.10.020

Chen Y, Li M, Li Y, Liu Y, Chen Y, Li H, Li L, Xu F, Jiang H, Chen L (2021) Hydroxyapatite modified sludge-based biochar for the adsorption of Cu^{2+} and Cd^{2+}: adsorption behavior and mechanisms. Biores Technol. https://doi.org/10.1016/j.biortech.2020.124413

Ding C, Cheng W, Wang X, Wu ZY, Sun Y, Chen C, Wang X, Yu SH (2016) Competitive sorption of Pb(II), Cu(II) and Ni(II) on carbonaceous nanofibers: a spectroscopic and modeling approach. J Hazard Mater. https://doi.org/10.1016/j.jhazmat.2016.04.002

Ding C, Cheng W, Wang X, Wu Z-Y, Sun Y, Chen C, Wang X, Yu S-H (2020) Corrigendum: competitive sorption of Pb(II), Cu(II) and Ni(II) on carbonaceous nanofibers: a spectroscopic and modeling approach. J Hazard Mater. https://doi.org/10.1016/j.jhazmat.2020.122118

Elkady M, Shokry H, Hamad H (2020) New activated carbon from mine coal for adsorption of dye in simulated water or multiple heavy metals in real wastewater. Materials. https://doi.org/10.3390/ma13112498

Fang X, Li J, Li X, Pan S, Zhang X, Sun X, Shen J, Han W, Wang L (2017) Internal pore decoration with polydopamine nanoparticle on polymeric ultrafiltration membrane for enhanced heavy metal removal. Chem Eng J. https://doi.org/10.1016/j.cej.2016.12.125

Feng N, Guo X, Liang S, Zhu Y, Liu J (2011) Biosorption of heavy metals from aqueous solutions by chemically modified orange peel. J Hazard Mater. https://doi.org/10.1016/j.jhazmat.2010.08.114

Gao LY, Deng JH, Huang GF, Li K, Cai KZ, Liu Y, Huang F (2019) Relative distribution of Cd^{2+} adsorption mechanisms on biochars derived from rice straw and sewage sludge. Biores Technol. https://doi.org/10.1016/j.biortech.2018.09.138

Gu YG, Li QS, Fang JH, He BY, Fu HB, Tong ZJ (2014) Identification of heavy metal sources in the reclaimed farmland soils of the pearl river estuary in China using a multivariate geostatistical approach. Ecotoxicol Environ Saf. https://doi.org/10.1016/j.ecoenv.2014.04.003

Gupta M, Gupta H, Kharat DS (2018) Adsorption of Cu(II) by low cost adsorbents and the cost analysis. Environ Technol Innov. https://doi.org/10.1016/j.eti.2018.02.003

Huang Z, Cheng C, Liu Z, Luo W, Zhong H, He G, Liang C, Li L, Deng L, Fu W (2019) Gemini surfactant: a novel flotation collector for harvesting of microalgae by froth flotation. Biores Technol. https://doi.org/10.1016/j.biortech.2018.12.106

Jia X, Fu T, Hu B, Shi Z, Zhu Y (2020) Identification of the potential risk areas for soil heavy metal pollution based on the source-sink theory. J Hazard Mater. https://doi.org/10.1016/j.jhazmat.2020.122424

Jin Y, Teng C, Yu S, Song T, Dong L, Liang J, Bai X, Liu X, Hu X, Qu J (2018) Batch and fixed-bed biosorption of Cd(II) from aqueous solution using immobilized Pleurotus ostreatus spent substrate. Chemosphere. https://doi.org/10.1016/j.chemosphere.2017.08.154

Jin Z, Deng S, Wen Y, Jin Y, Pan L, Zhang Y, Black T, Jones KC, Zhang H, Zhang D (2019) Application of Simplicillium chinense

for Cd and Pb biosorption and enhancing heavy metal phytoremediation of soils. Sci Total Environ. https://doi.org/10.1016/j.scitotenv.2019.134148

Júnior OK, Gurgel LVA, de Freitas RP, Gil LF (2009) Adsorption of Cu(II), Cd(II), and Pb(II) from aqueous single metal solutions by mercerized cellulose and mercerized sugarcane bagasse chemically modified with EDTA dianhydride (EDTAD). Carbohyd Polym. https://doi.org/10.1016/j.carbpol.2009.02.016

Jurado-Sánchez B, Sattayasamitsathit S, Gao W, Santos L, Fedorak Y, Singh VV, Orozco J, Galarnyk M (2015) Self-propelled activated carbon Janus micromotors for efficient water purification. Small. https://doi.org/10.1002/smll.201402215

Kai C, Wei W, Biying R, Jing He (2017) A phytic acid modified $CoFe_2O_4$ magnetic adsorbent with controllable morphology, excellent selective adsorption for dyes and ultra-strong adsorption ability for metal ions. Chem Eng J. https://doi.org/10.1016/j.cej.2017.08.009

Kerr JG, Cooke CA (2017) Erosion of the Alberta badlands produces highly variable and elevated heavy metal concentrations in the Red Deer River, Alberta. Science of The Total Environment. https://doi.org/10.1016/j.scitotenv.2017.04.037

Kołodyńska D, Hubicka H, Hubicki Z (2008) Sorption of heavy metal ions from aqueous solutions in the presence of EDTA on monodisperse anion exchangers. Desalination. https://doi.org/10.1016/j.desal.2007.06.022

Kołodyńska D, Krukowska J, Thomas P (2017) Comparison of sorption and desorption studies of heavy metal ions from biochar and commercial active carbon. Chem Eng J. https://doi.org/10.1016/j.cej.2016.08.088

Krylova V, Dukštienė N (2019) The structure of PA-Se-S-Cd composite materials probed with FTIR spectroscopy. Appl Surf Sci. https://doi.org/10.1016/j.apsusc.2018.11.121

Lasheen MR, Ammar NS, Ibrahim HS (2012) Adsorption/desorption of Cd(II), Cu(II) and Pb(II) using chemically modified orange peel: equilibrium and kinetic studies. Solid State Sci. https://doi.org/10.1016/j.solidstatesciences.2011.11.029

Lessa EF, Gularte MS, Garcia ES, Fajardo AR (2017) Orange waste: a valuable carbohydrate source for the development of beads with enhanced adsorption properties for cationic dyes. Carbohyd Polym. https://doi.org/10.1016/j.carbpol.2016.10.019

Li X, Tang Y, Cao X, Lu D, Luo F, Shao W (2008) Preparation and evaluation of orange peel cellulose adsorbents for effective removal of cadmium, zinc, cobalt and nickel. Colloids Surf, A. https://doi.org/10.1016/j.colsurfa.2007.11.031

Li Z, Ge Y (2018) Application of lignin and its derivatives in adsorption of heavy metal ions in water: a review. ACS Sustainable Chemistry & Engineering. https://doi.org/10.1021/acssuschemeng.8b01345

Lim SF, Zheng YM, Zou SW, Chen JP (2008) Characterization of copper adsorption onto an alginate encapsulated magnetic sorbent by a combined FT-IR, XPS and mathematical modeling study. Environmental Science and Technology. https://doi.org/10.1021/es7021889

Ling C, Liu FQ, Xu C, Chen TP, Li AM (2013) An integrative technique based on synergistic coremoval and sequential recovery of copper and tetracycline with dual-functional chelating resin: roles of amine and carboxyl groups. ACS Appl Mater Interfaces. https://doi.org/10.1021/am403491b

Liu C, Huu Hao N, Guo W, Tung K-L (2012) Optimal conditions for preparation of banana peels, sugarcane bagasse and watermelon rind in removing copper from water. Biores Technol. https://doi.org/10.1016/j.biortech.2012.06.004

Ma L, Wang L, Tang J, Yang Z (2017) Arsenic speciation and heavy metal distribution in polished rice grown in Guangdong Province, Southern China. Food Chemistry. https://doi.org/10.1016/j.foodchem.2017.04.097

Mei Y, Xu J, Zhang Y, Li B, Fan S, Xu H (2021) Effect of Fe-N modification on the properties of biochars and their adsorption behavior on tetracycline removal from aqueous solution. Biores Technol. https://doi.org/10.1016/j.biortech.2021.124732

Memon JR, Memon SQ, Bhanger MI, Memon GZ, El-Turki A, Allen GC (2008) Characterization of banana peel by scanning electron microscopy and FT-IR spectroscopy and its use for cadmium removal. Colloid Surf. B-Biointerfaces. https://doi.org/10.1016/j.colsurfb.2008.07.001

Mia S, Dijkstra FA, Singh B (2017) Aging induced changes in biochar's functionality and adsorption behavior for phosphate and ammonium. Environ Sci Technol. https://doi.org/10.1021/acs.est.7b00647

Módenes AN, de Abreu Pietrobelli JMT, dos Santos GHF, Borba CE, da Silva Sá Ravagnani MA, Espinoza-Quiñones FR (2018) Multi-component mathematical model based on mass transfer coefficients for prediction of the Zn and Cd ions biosorption data by E. densa in a continuous system. Journal of Environmental Chemical Engineering. https://doi.org/10.1016/j.jece.2018.08.001

Moreno-Pirajan JC, Giraldo L (2012) Heavy metal ions adsorption from wastewater using activated carbon from orange peel. E-Journal of Chemistry. https://doi.org/10.1155/2012/383742

Mourya A, Mazumdar B, Sinha SK (2019) Determination and quantification of heavy metal ion by electrochemical method. J Environ Chem Eng. https://doi.org/10.1016/j.jece.2019.103459

Németh G, Mlinárik L, Török Á (2016) Adsorption and chemical precipitation of lead and zinc from contaminated solutions in porous rocks: possible application in environmental protection. J Afr Earth Sc. https://doi.org/10.1016/j.jafrearsci.2016.04.022

Pathak PD, Mandavgane SA, Kulkarni BD (2015) Fruit peel waste as a novel low-cost bio adsorbent. Rev Chem Eng. https://doi.org/10.1515/revce-2014-0041

Pereira FV, Gurgel LVA (2010) Removal of Zn^{2+} from aqueous single metal solutions and electroplating wastewater with wood sawdust and sugarcane bagasse modified with EDTA dianhydride (EDTAD). J Hazard Mater. https://doi.org/10.1016/j.jhazmat.2009.11.115

Sameena, N.Malik, Shahabaz, M.Khan, Prakash, C.Ghosh, Atul, N.Vaidya, Gajanan (2019) Microscopic morphology and seasonal variation of health effect arising from heavy metals in PM2.5 and PM10: one-year measurement in a densely populated area of urban Beijing. Atmospheric Research. https://doi.org/10.1016/j.atmosres.2018.04.027

Singh SA, Shukla SR (2015) Adsorptive removal of cobalt ions on raw and alkali-treated lemon peels. Int J Environ Sci Technol. https://doi.org/10.1007/s13762-015-0801-6

Surgutskaia NS, Martino AD, Zednik J, Ozaltin K, Lovecká L, Bergerová ED, Kimmer D, Svoboda J, Sedlarik V (2020) Efficient Cu^{2+}, Pb^{2+} and Ni^{2+} ion removal from wastewater using electrospun DTPA-modified chitosan/polyethylene oxide nanofibers. Sep Purif Technol. https://doi.org/10.1016/j.seppur.2020.116914

Tan IAW, Chan JC, Hameed BH, Lim LLP (2016) Adsorption behavior of cadmium ions onto phosphoric acid-impregnated microwave-induced mesoporous activated carbon. Journal of Water Process Engineering. https://doi.org/10.1016/j.jwpe.2016.10.007

Vilardi G, Di Palma L, Verdone N (2018) Heavy metals adsorption by banana peels micro-powder: equilibrium modeling by non-linear models. Chin. Chemical Engineering Journal. https://doi.org/10.1016/j.cjche.2017.06.026

Villen-Guzman M, Cerrillo-Gonzalez MM, Paz-Garcia JM, Rodriguez-Maroto JM, Arhoun B (2021) Valorization of lemon peel waste as biosorbent for the simultaneous removal of nickel and cadmium from industrial effluents. Environ Technol Innov. https://doi.org/10.1016/j.eti.2021.101380

Wang X, Chen QR, Lu X (2014) Pectin extracted from apple pomace and citrus peel by subcritical water. Food Hydrocolloids. https://doi.org/10.1016/j.foodhyd.2013.12.003

Xu H, Hu X, Chen Y, Li Y, Zhang R, Tang C, Hu X (2021) Cd(II) and Pb(II) absorbed on humic acid-iron-pillared bentonite: kinetics, thermodynamics and mechanism of adsorption. Colloids Surf A : Physicochemical and Engineering Aspects. https://doi.org/10.1016/j.colsurfa.2020.126005

Yang GX, Jiang H (2014) Amino modification of biochar for enhanced adsorption of copper ions from synthetic wastewater. Water Res. https://doi.org/10.1016/j.watres.2013.09.050

Yong YA, Xue YA, B MH (2020) Beyond mere pollution source identification: Determination of land covers emitting soil heavy metals by combining PCA/APCS, GeoDetector and GIS analysis. CATENA. https://doi.org/10.1016/j.catena.2019.104297

Yuan G, Tian Y, Liu J, Tu H, Liao J, Yang J, Yang Y, Wang D, Liu N (2017) Schiff base anchored on metal-organic framework for Co (II) removal from aqueous solution. Chem Eng J. https://doi.org/10.1016/j.cej.2017.06.024

Zhang J, Xu Y, Wu Y, Hu S, Zhang Y (2019a) Dynamic characteristics of heavy metal accumulation in the farmland soil over Xiaoqinling gold-mining region, Shaanxi, China. Environmental Earth Sciences. https://doi.org/10.1007/s12665-018-8013-2

Zhang W, Deng Q, He Q, Song J, Zhang S, Wang H, Zhou J, Zhang H (2018) A facile synthesis of core-shell/bead-like poly (vinyl alcohol)/alginate@PAM with good adsorption capacity, high adaptability and stability towards Cu(II) removal. Chem Eng J. https://doi.org/10.1016/j.cej.2018.06.129

Zhang W, Lan Y, Ma M, Chai S, Zuo Q, Kim K-H, Gao Y (2020a) A novel chitosan–vanadium-titanium-magnetite composite as a superior adsorbent for organic dyes in wastewater. Environ Int. https://doi.org/10.1016/j.envint.2020.105798

Zhang W, Song J, He Q, Wang H, Lyu W, Feng H, Xiong W, Guo W, Wu J, Chen L (2020b) Novel pectin based composite hydrogel derived from grapefruit peel for enhanced Cu(II) removal. J Hazard Mater. https://doi.org/10.1016/j.jhazmat.2019.121445

Zhang XH, Zhang ZC, Deng ZH, Li S, Wu QP, Kang ZX (2019b) Precision grinding of silicon nitride ceramic with laser macro-structured diamond wheels. Opt Laser Technol. https://doi.org/10.1016/j.optlastec.2018.08.021

Zhao FP, Repo E, Yin DL, Sillanpaa MET (2013) Adsorption of Cd(II) and Pb(II) by a novel EGTA-modified chitosan material: kinetics and isotherms. J Colloid Interface Sci. https://doi.org/10.1016/j.jcis.2013.07.062

Zheng X, Zhou Y, Liu X, Fu X, Peng H, Lv S (2020) Enhanced adsorption capacity of MgO/N-doped active carbon derived from sugarcane bagasse. Biores Technol. https://doi.org/10.1016/j.biortech.2019.122413

Zhou G, Luo J, Liu C, Chu L, Crittenden J (2018) Efficient heavy metal removal from industrial melting effluent using fixed-bed process based on porous hydrogel adsorbents. Water Res. https://doi.org/10.1016/j.watres.2017.12.067

Zhu YH, Hu J, Wang JL (2012) Competitive adsorption of Pb(II), Cu(II) and Zn(II) onto xanthate-modified magnetic chitosan. Journal of Hazardous Materials. https://doi.org/10.1016/j.jhazmat.2012.04.026